Proceedings of the 4th International Conference on Functional Materials and Civil Engineering
DOI: 10.54254/2755-2721/2026.38490

Research Progress in Channel-Selective Dealumination of Mordenite for Humid Direct Air Capture of CO_2

Shiran Cheng

Department of Energy, Environmental and Chemical Engineering, Washington University in St. Louis, St. Louis, USA
shirancheng24@gmail.com

Abstract. Direct air capture (DAC) of CO_2 requires physisorbents that retain their selectivity in the presence of atmospheric water vapour. For zeolites the principal framework-level lever on water affinity is the Si/Al ratio, and the only post-synthetic route to raising it is dealumination. Mordenite (MOR) has become a focus of this effort because its 8-membered-ring (8-MR) side pocket, rather than its 12-membered-ring (12-MR) main channel, governs CO_2 uptake at 400 ppm, so dealumination must be directed at one channel while preserving the other. This paper reviews progress in channel-selective dealumination of MOR and in its evaluation for humid DAC. The underlying principles are summarised first: pore topology and T-site distribution, the evaluation criteria appropriate to trace-concentration humid conditions, the dual role of extra-framework cations as adsorption sites and as protecting agents, and the competing effects that dealumination produces. Four families of channel-selective strategy are then reviewed by category — conventional acid leaching and chelation, size-gated in-situ proton generation, cation site-protection combined with steaming, and silylation capping — together with recent progress in humid CO_2 adsorption performance. The strategies are compared in tabular form, and the characterisation methods appropriate to demonstrating channel selectivity are summarised. Finally, the remaining challenges and prospects for this field are outlined.

Keywords: mordenite, dealumination, direct air capture, side pocket, humid CO_2 adsorption

1. Introduction

Atmospheric CO_2 concentration has passed 425 ppm, and mitigation pathways consistent with limiting warming to 1.5 °C now require gigatonne-scale carbon dioxide removal in addition to emissions reduction. Direct air capture (DAC) is among the few removal technologies whose siting is independent of point sources, which makes it applicable to distributed and historical emissions that no point-source capture can address. Its deployment is at present limited by cost, which remains above 500 USD per tonne against a widely cited target near 100 USD per tonne, and the dominant contributor to that cost is the energy required to regenerate the sorbent [1]. A practical DAC sorbent must therefore capture CO_2 at 425 ppm, release it below 100 °C, and retain both properties in ambient air, where the partial pressure of water vapour exceeds that of CO_2 by two orders of magnitude. Meeting all three requirements simultaneously is the central materials challenge of the

© 2026 The Authors. This is an open access article distributed under the terms of the Creative Commons Attribution License 4.0 (https://creativecommons.org/licenses/by/4.0/).

DOI: 10.54254/2755-2721/2026.38490

field, and tolerance to water rather than raw capacity is the constraint that governs sorbent design [2, 3].

Zeolites are crystalline aluminosilicates in which substitution of framework Si^{4+} by Al^{3+} generates a negative framework charge balanced by an extra-framework cation. These cations interact electrostatically with the CO_2 quadrupole moment, conferring a CO_2 selectivity that no non-polar surface reproduces, but they bind water more strongly still through its permanent dipole; lowering framework polarity by raising the Si/Al ratio is the established response, and for an already-crystallised material the only route to a higher ratio is post-synthetic dealumination [4]. Mordenite (MOR) has become a focus of this effort because it contains two channel systems of sharply different size, a 12-membered-ring (12-MR) main channel and an 8-MR side pocket. Fu, Park and Davis demonstrated in 2022 that at low concentration CO_2 adsorbs almost exclusively at Na^+ within the side pocket [5], and Kong et al. subsequently achieved a breakthrough time of 2364 min g^{-1} at 400 ppm by biasing framework Al toward that pocket during synthesis [6], while Lee et al. established crystallographically in 2025 how cation electronegativity and hydration energy determine which cations occupy it [7]. Because the pocket rather than the main channel carries the adsorption, dealumination must be directed at one channel while preserving the other, and several routes to such spatial control have been reported: Xue et al. achieved 86% removal of 12-MR Brønsted sites against 4% of 8-MR sites by steaming a cation-protected MOR [8], Xu et al. showed that steaming the sodium form preferentially removes 12-MR framework Al [9], and Xing et al. reported in 2025 a persulfate route generating protons in situ within the 12-MR alone [10]. Evaluation has advanced in parallel, Benamar et al. demonstrating in 2024 that high-resolution argon physisorption resolves the side pocket and main channel as separate micropore populations [11], and Lyadov and Lusardi establishing in 2025 the metrics appropriate to humid DAC conditions [3].

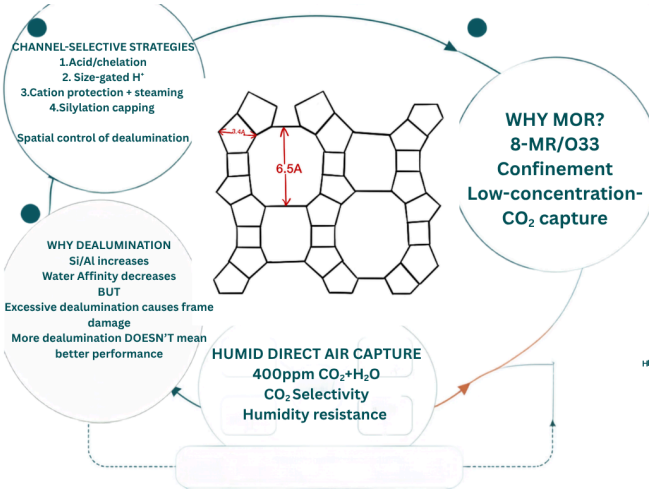

Figure 1. Overview of channel-selective dealumination of mordenite for humid direct air capture. Ambient air at 400 ppm CO_2 with competing water vapour sets the performance requirement (bottom); CO_2 adsorbs predominantly at Na^+ in the 8-MR side pocket, whose confinement governs uptake at trace concentration (right); dealumination raises the Si/Al ratio and lowers water affinity but damages the framework when excessive (left); and four families of channel-selective strategy have been developed to direct aluminium removal spatially (top). Centre: MOR framework viewed along the c axis, showing the 12-MR main channel (6.5 × 7.0 Å); the 8-MR side pockets (3.4 × 4.8 Å) run along b, perpendicular to the plane shown

DOI: 10.54254/2755-2721/2026.38490

This paper reviews research progress in channel-selective dealumination of mordenite and its application to humid direct air capture. Four families of strategy — conventional acid leaching and chelation, size-gated in-situ proton generation, cation site-protection combined with steaming, and silylation capping — are surveyed by category and compared in terms of the channel selectivity achieved, the textural cost incurred, and the characterisation methods on which each claim rests, together with recent progress in humid CO_2 adsorption performance and the challenges that remain open. The scope and organisation of this review are summarised in Figure 1.

2. Principles

2.1. Pore topology and T-site distribution

MOR comprises a 12-MR main channel of 6.5–7.0 × 7.0 Å along the c axis, a narrow 8-MR channel of 2.6 × 5.7 Å also along c, and 8-MR side pockets of 3.4 × 4.8 Å along b connecting the two (Figure 2) [9, 11]. Argon physisorption at 87 K resolves the pockets and the main channel as separate micropore populations of mean diameter 0.42 and 0.57 nm, the pockets accounting for approximately 25% of total micropore volume in a parent H-MOR [11]. Framework aluminium occupies four crystallographically distinct T sites: T1 and T2 lie in the main channel, whereas T3 and T4 sit in the four-membered rings forming the side-pocket communication windows and constitute the less stable pair [11]. The cation position designated O33 lies within the side pocket and is associated with T3. Because CO_2 adsorption at trace concentration occurs predominantly at O33, dealumination intended to improve humid performance must be directed at T1 and T2 while preserving T3 and T4.

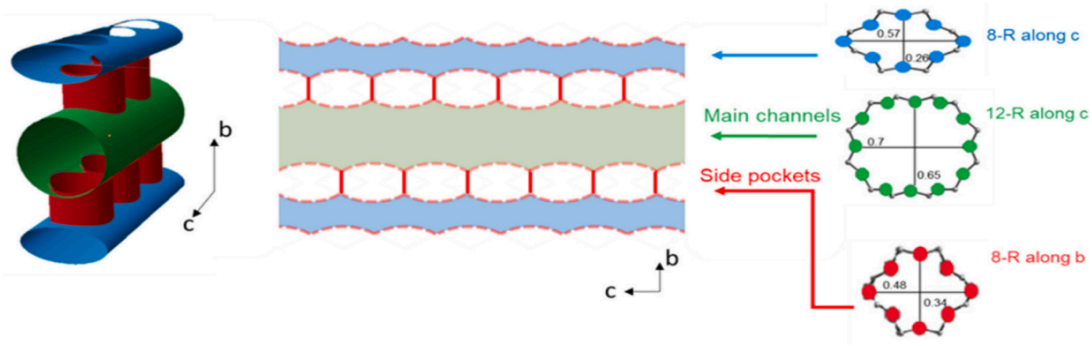

Scheme 1. Schematic representation of the porous system of the **MOR** framework.

Figure 2. Pore system of the MOR framework. The 12-MR main channels (0.65 × 0.70 nm) and the 8-MR channels (0.26 × 0.57 nm) both run along the crystallographic c axis and are connected by 8-MR side pockets (0.34 × 0.48 nm) along b. Reprinted from ref. [11] with permission from Elsevier

2.2. Evaluation criteria under trace-concentration humid conditions

At flue-gas concentrations of 10–15% CO_2 the working capacity is set by the difference between the adsorption and desorption branches of a flat, high-loading isotherm, and raw capacity is the governing design objective. At 425 ppm the operative region is the initial, near-linear portion of the isotherm, whose slope is determined by the strength of the strongest available sites rather than by total pore volume. Rankings obtained at high pressure therefore do not transfer to trace concentration.

DOI: 10.54254/2755-2721/2026.38490

Humidity imposes a further constraint. Lyadov and Lusardi reported in 2025 that a dry 400 ppm capacity of 0.26 mmol g^{-1} on 13X collapsed to 0.0175 mmol g^{-1} at only 5% relative humidity, a loss of roughly 93%, while K-MER3.6 fell essentially to zero [3]. Under equilibrium conditions at DAC concentration, humid selectivity therefore possesses limited discriminating power. Discrimination is recovered under cycling: with mild 100 °C regeneration, K-MER3.6 retained 73% of its dry capacity over five humid cycles whereas 13X retained only 47%. Cyclic working capacity and retention under mild regeneration are consequently the appropriate performance metrics for this regime. Chemisorbed carbonate formation constitutes an additional failure mode, requiring temperatures above 250 °C for complete regeneration, so candidate materials should also be examined in the carbonate region of the infrared spectrum [3].

2.3. Dual role of extra-framework cations

The charge-to-size ratio and hydration energy of a cation determine whether it can occupy the 8-MR environment. Lee et al. verified this relationship by synchrotron Rietveld refinement, finding Cs^+ located predominantly near the 8-MR while strongly hydrated Sr^{2+} and Cd^{2+} remained hydrated in the centre of the 12-MR channel [7]. Extrapolation along the alkali series predicts Li^+ to be the strongest CO_2 binder, a prediction supported by density functional theory [12] and by calorimetry on alkali-exchanged ferrierites [13].

The same cations serve a second function during dealumination. Hydrolysis of a framework Al–O bond requires a proton, so a site whose Brønsted proton has been replaced by a metal cation possesses no local acid source and cannot initiate dealumination [14]. Nagano et al. provided physical evidence for this occupancy: the activation energy for xenon exchange between main channel and side pocket is 21 kJ mol^{-1} in Na-MOR against 18 kJ mol^{-1} in H-MOR, and the apparent pocket size derived from the ^{129}Xe chemical shift is smaller in the sodium form, indicating that Na^+ resides at or near the pocket entrance [15]. A practical consequence is that the protecting cation and the final working cation need not be the same species, so a complete route comprises protection, treatment and a final ion exchange.

2.4. Competing effects of dealumination

Raising the Si/Al ratio lowers framework polarity and reduces water affinity, and hydrophobicity correlates directly with the SiO_2/Al_2O_3 ratio across a wide range of materials [4]. The same treatment, however, produces four effects acting in the opposite direction. Dealumination leaves a hydrophilic silanol nest at each vacated T site; Yoshioka et al. measured water uptake rising from 12% to 13% after acid treatment and falling to 6.2% only after a subsequent defect-repair step in which amorphous silicon migrates into the vacancies [16]. Each aluminium removed also removes a charge-compensating cation, so the density of CO_2 binding sites falls together with the density of hydrophilic sites. Liberated aluminium does not necessarily leave the crystal, and retained extra-framework aluminium (EFAl) blocks side pockets physically [9]. Finally, dealumination enlarges the pocket itself: Nagano et al. found the rotational barrier of adsorbed methane within the pocket falling from 5.0 to 1.0 kJ mol^{-1} between Si/Al 8.6 and 40, while the main-channel barrier remained essentially unchanged at 0.53 and 0.45 kJ mol^{-1} [15]. Optimising the degree of dealumination therefore involves balancing these effects rather than maximising the Si/Al ratio.

DOI: 10.54254/2755-2721/2026.38490

3. Research progress

3.1. Conventional acid leaching and chelation

Liquid-phase dealumination proceeds in two steps: solution acidity hydrolyses framework Al–O bonds, converting tetrahedral framework Al into detached octahedral EFAl, after which a chelating agent, if present, complexes the freed Al^{3+} and removes it from the pore system [14]. The reagents surveyed in this section are compared in Table 1 in terms of the acidity, denticity and anion size that govern these two steps.

In 2000, Giudici, Kouwenhoven and Prins compared nitric and oxalic acid on MOR at 100 °C and found that oxalic acid extracted aluminium more rapidly even at low concentration, but that at equal bulk Si/Al nitric acid left almost no EFAl whereas approximately half the aluminium remained octahedrally coordinated after oxalic acid treatment [17], establishing that liberation and removal proceed on different timescales.

In 2017, Reule, Sawada and Semagina treated MOR with a nitric acid series of increasing severity and, by combining ^{27}Al and ^{29}Si NMR with catalytic testing in dimethyl ether carbonylation, identified the selectively removed positions as T3 and T4 on the four-membered ring [18]. The mildest treatment improved activity while progressively severe treatment was detrimental.

In 2022, Babić et al. treated CHA, MFI and LTL zeolites with chromic acid and found that, despite an exceptional pKa of −0.7, the reagent removed almost no aluminium from 8-MR CHA or 10-MR MFI while removing 45% from 12-MR LTL, attributing the difference to the 0.56 nm size of the dichromate anion [19], thereby demonstrating that the anion rather than the proton sets whatever size gate exists in bulk acid treatment.

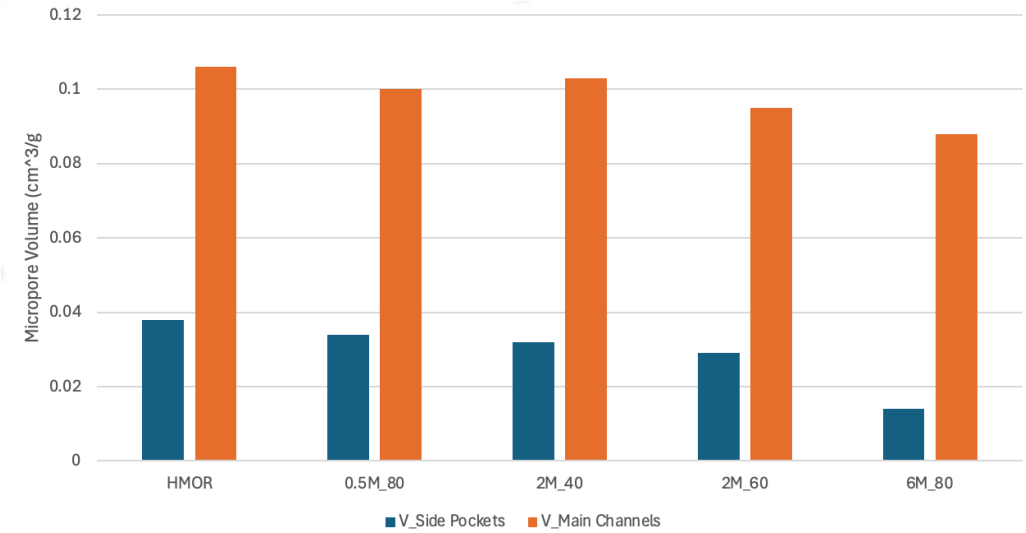

Figure 3. Side-pocket (VSP) and main-channel (VLM) micropore volumes of MOR after nitric acid leaching of increasing severity, showing preservation of the side pocket under moderate conditions and its collapse under severe treatment. Plotted from data in ref. [11]

In 2024, Benamar, Sachse, Miqueu and Batonneau-Gener prepared a nitric acid series on MOR and analysed it by high-resolution argon physisorption at 87 K with n-nonane pre-adsorption, resolving the side-pocket and main-channel micropore populations separately for the first time [11]. At 0.5 M and 343 K the side-pocket volume fell only from 0.038 to 0.034 $cm^3\ g^{-1}$ while the main-channel population fell from 0.106 to 0.100 $cm^3\ g^{-1}$ and broadened toward larger diameters; at 6 M

DOI: 10.54254/2755-2721/2026.38490

and 353 K the pocket volume collapsed by more than 60% to 0.014 $cm^3\ g^{-1}$ against a 16% loss in the main channel (Figure 3). They further defined an accessibility index φ_Ar quantifying micropore enlargement.

In 2025, Xu et al. prepared a series of dealuminated MOR samples of graded severity and showed that mild acid removes only EFAl, opening the side pocket and raising the count of accessible strong acid sites with carbonylation activity improving by 40%, whereas concentrated acid removes framework Al and preferentially destroys the Brønsted sites within the pocket [20].

In 2025, Hu, Qie and co-workers prepared MOR, Y and Beta samples treated with oxalic acid or EDTA followed by ammonium hydroxide, and evaluated their CO_2 adsorption under humid conditions [21]. On MOR the post-treatment CO_2/H_2O selectivity ranked oxalic acid 0.221, untreated parent 0.189 and EDTA 0.154, the EDTA-treated sample showing a BET surface area collapsing from 330 to 1.09 $m^2\ g^{-1}$ through trapped aluminium–EDTA complexes; on cage-type Y the ranking reversed, oxalic acid producing the greater damage. They also showed that a mild 0.1 M ammonium hydroxide step clears octahedral aluminium without attacking framework aluminium.

Related work on other frameworks has extended the reagent range. In 2007, Fan et al. treated steamed HZSM-5 with citric acid and observed realumination, extra-framework aluminium reinserting into framework defect sites; prior steaming was reported to be a precondition, since the lattice defects it generates are required for citric acid to act in this direction [22].

3.2. Size-gated in-situ proton generation

In 2025, Xing et al. developed a route that controls not where the proton acts but where it is generated [10]. Ammonium persulfate, at 5.7 Å, enters the 12-MR window but neither the 8-MR window nor the side pocket; it is inert at room temperature and decomposes only at 80 °C, whereupon sulfate radicals hydrolyse water to release protons in situ. Synchrotron X-ray diffraction with Rietveld refinement located the persulfate sulfur 3.68 Å from T2 and 3.78 Å from T1 but 7.69 Å from T3, and no dealumination occurred under dry nitrogen, confirming that water is required for proton generation. The treated material showed 12-MR Brønsted sites reduced by 30% against 8-MR sites reduced by 3%, with bulk, framework and surface Si/Al ratios in agreement at 10.20, 10.06 and 10.98, and delivered improved stability in dimethyl ether carbonylation. The authors noted that efficiency is limited to approximately 25% by the short radical lifetime, optimisation raising 12-MR removal only to about 40%.

3.3. Cation site-protection combined with steaming

In 2013, Xue, Huang, Zhan, Ma and Shen prepared a selectively dealuminated MOR by blocking the 12-MR with pyridine, whose 0.585 nm diameter admits it to the 12-MR but not the 8-MR, placing Na^+ in the pocket with dilute NaOH, and then steaming at 750 °C [8]. Pyridine-preadsorbed NH_3-TPD showed 8-MR acid sites falling from 0.76 to 0.73 mmol g^{-1} against 12-MR sites falling from 0.81 to 0.11 mmol g^{-1}, corresponding to 4% and 86% removal respectively, at a cost of 12% micropore volume with mesopore generation. The material showed markedly improved stability in dimethyl ether carbonylation.

In 2015, Armitage and Sunley patented a milder variant in which a monovalent metal loaded onto MOR spontaneously occupies the 8-MR Brønsted site before steaming at 500 °C, evidenced by loss of the 3590 cm^{-1} infrared band while the 3610 cm^{-1} band remains [23]. The patent reports no quantitative acid-site characterisation.

DOI: 10.54254/2755-2721/2026.38490

In 2022, Xu, Lv, Zhu and co-workers prepared a full series of steamed MOR samples in both sodium and proton forms at 673, 773 and 873 K, and characterised them by XRD, N_2 physisorption, ^{29}Si and ^{27}Al MAS NMR, NH_3-TPD and DRIFTS [9]. Deconvoluting the 3610 and 3592 cm^{-1} hydroxyl bands and combining the ratio with NH_3-TPD, they found that Na-MOR steamed at 773 K showed 8-MR Brønsted sites rising from 0.53 to 0.68 mmol g^{-1} alongside 12-MR sites falling from 0.52 to 0.50 mmol g^{-1}, with micropore volume increasing from 0.179 to 0.189 cm^3 g^{-1} and relative crystallinity retained at 89%. The rise in 8-MR site count reflects the opening of pockets previously blocked by amorphous material rather than an increase in aluminium content, and methyl acetate productivity rose correspondingly from 0.23 to 0.33 g g^{-1} h^{-1}, a 1.7-fold increase in total yield. Steaming the proton form under the same conditions produced the opposite distribution, the 8-MR/12-MR band ratio falling from 1.01 to 0.45, together with reduced crystallinity and micropore volume.

In 2023, Bai, Zhang, Liu and co-workers studied the dealumination mechanism of H-MOR under high-temperature hydrothermal treatment at 4 mol% steam by solid-state NMR, reporting the 8-MR/12-MR Brønsted concentration ratio rising from approximately 1.15 to 1.5 and the Si–OH proton resonance increasing monotonically with steaming severity [24].

3.4. Silylation capping

In 2022, Liu, Zeng, Sun and co-workers prepared a MOR in which 12-MR acid sites were selectively deactivated by trimethylchlorosilane silylation [25]. At 6.9 Å the reagent enters the 12-MR but neither the 8-MR nor the side pocket, and caps the Brønsted proton while leaving aluminium in the framework. The material showed no measurable micropore loss and improved carbonylation selectivity. Because the aluminium is retained and organosilicon residue is added to the pore system, the method modifies acidity rather than framework composition, and is included here as a boundary case within the size-discrimination family.

Because the treatment is confined to the 12-MR, its consequences for water adsorption have not been evaluated. Capping a Brønsted proton with a trimethylsilyl group removes a hydrophilic site but introduces an organosilicon residue whose stability under the humid temperature-swing cycling of DAC is unknown, and the aluminium responsible for framework polarity remains in place. Silylation is therefore untested for the application considered here, although it provides the cleanest available demonstration that a size-selected reagent can be confined to the main channel alone.

3.5. Progress in humid CO_2 adsorption performance

In 2022, Fu, Park and Davis established the location of the CO_2 adsorption site in MOR by blocking the 12-MR channel with pyridine and correlating Na^+ site populations with CO_2 uptake across a composition series, showing that Na^+ at the O33 site within the side pocket accounts for the majority of low-concentration uptake, a secondary intersection site contributing approximately 20% and Na^+ in the open 12-MR channel contributing essentially nothing [5].

In 2024, Chen, Yaghi and co-workers reported amine-functionalised MOF-808 variants in which 400 ppm CO_2 uptake nearly doubled at 50% relative humidity through bicarbonate chemistry, demonstrating that water can be exploited rather than merely tolerated [26].

In 2025, Kong et al. prepared MOR samples using organic structure-directing agents that bias framework Al substitution toward the 8-MR pocket at nearly constant Si/Al, decoupling cation location from cation count, and confirmed by grand-canonical Monte Carlo simulation that CO_2 at

DOI: 10.54254/2755-2721/2026.38490

0.0004 bar occupies the pocket almost exclusively; the material achieved a breakthrough time of 2364 min g^{-1} at 400 ppm [6].

In 2025, Lee et al. prepared a series of cation-exchanged mordenites spanning a wide range of ionic size and charge and, by synchrotron powder diffraction with Rietveld refinement, correlated extra-framework cation electronegativity with both cation position and CO_2 adsorption capacity [7].

In 2025, Lyadov and Lusardi characterised K-MER and 13X under genuine DAC conditions in both equilibrium and temperature-swing cycling modes, establishing the humidity sensitivity and cycling behaviour described in Section 2.2 [3].

In 2026, Liu et al. reported Li^+-exchanged mordenite combining aperture widening with strong polarisation, raising the 400 ppm capacity from 1.02 to 1.42 mmol g^{-1} [27].

4. Comparison

4.1. Reagent parameters in liquid-phase dealumination

The reagents used in liquid-phase dealumination differ in three properties that together determine their behaviour. Acid strength sets the rate at which framework Al–O bonds are hydrolysed; denticity determines whether the liberated Al^{3+} is chelated and carried out of the pore system or left behind as EFAl; and anion size determines whether the reagent can reach a given channel at all. Table 1 collects these parameters alongside the effects reported on MOR and on other frameworks, so that each reported outcome can be read against the reagent property responsible for it.

Table 1. Acidity, denticity, anion size and reported effects of reagents used in liquid-phase dealumination

Reagent (pKa_1 / denticity / anion size)	Effect on MOR	Effect on other frameworks
Nitric acid (−1.4 / none / small)	Degree-controllable; T3/T4 selective [18]; side pocket preserved at 0.5 M, lost >60% at 6 M [11]	Common baseline
Oxalic acid (1.25 / 2 / small)	Highest CO_2/H_2O ratio, 0.221 [21]; ~half of Al retained as EFAl after water washing [17]	More damaging than EDTA on cage-type Y [21]
Citric acid (3.13 / 3 / intermediate)	Not reported	Causes realumination on steamed HZSM-5 [22]
EDTA (insoluble as free acid / 6 / large)	S_{BET} 330 → 1.09 m^2 g^{-1}; CO_2/H_2O 0.154 [21]	Less damaging than oxalic acid on Y [21]
Chromic acid (−0.7 / none / 0.56 nm)	Not reported	45% Al removed from 12-MR LTL; negligible from 8-MR CHA and 10-MR MFI [19]

Three patterns are apparent in Table 1. First, acid strength alone does not predict the extent of dealumination: chromic acid, the strongest reagent listed at a pKa of −0.7, removed almost no aluminium from 8-MR CHA or 10-MR MFI while removing a substantial fraction from 12-MR

DOI: 10.54254/2755-2721/2026.38490

LTL, the discrimination following the 0.56 nm size of the dichromate anion rather than the acidity of the proton [19]. Second, denticity governs removal rather than liberation: oxalic acid extracts aluminium from MOR more rapidly than nitric acid, yet leaves approximately half of it octahedrally coordinated within the pore system, whereas nitric acid leaves almost none [17]. Third, the same reagent may act in opposite directions on different frameworks — EDTA is less damaging than oxalic acid on cage-type Y but collapses the surface area of MOR through trapped aluminium–EDTA complexes [21], and citric acid, rather than removing aluminium, reinserts it into framework defects on steamed HZSM-5 [22]. Reagent selection therefore cannot be made on acidity alone, and must be matched to both the pore topology and the prior treatment history of the material.

4.2. Comparison of channel-selective strategies

The four strategy families differ in the physical property on which their selectivity rests, and consequently in what each can and cannot achieve. Table 2 sets them side by side in terms of that basis of selectivity, the channel discrimination reported, the textural cost incurred and the principal limitation of each.

Table 2. Reported channel selectivity, textural cost and limitations of the four strategy families. Acid-site data are quoted for the persulfate and site-protection routes and micropore-volume data for acid leaching, as reported in the respective studies

Strategy (basis of selectivity)	Reported outcome	Textural cost	Limitation
Acid leaching and chelation (degree of treatment)	Side pocket preserved at 0.5 M, lost >60% at 6 M [11]	Route- and severity-dependent	Site preference toward T3/T4 [18]
In-situ proton generation (where the proton forms)	12-MR −30%, 8-MR −3% [10]	Not significant	~25% efficiency; ceiling near 40%
Cation protection and steam (occupancy of the protected site)	12-MR −86%, 8-MR −4% [8]; 8-MR +28% [9]	12% micropore volume [8]	Requires prior cation exchange
Silylation capping (reagent size)	12-MR sites deactivated [25]	None measurable	Aluminium retained; residue added

Comparing the four families, cation site-protection combined with steaming has achieved the largest quantified channel discrimination, at a measurable cost to micropore volume and with the additional requirement of a prior exchange step. In-situ proton generation gives the most complete structural evidence and the smallest textural cost but is limited in extent by radical lifetime. Conventional acid leaching offers control over the degree of dealumination and, in the moderate regime, preferential consumption of the main channel, but its direction reverses at higher severity. Silylation preserves texture completely but modifies acidity rather than framework composition.

4.3. Characterisation of channel selectivity

Bulk composition alone cannot detect framework dealumination, since converting framework Al to EFAl conserves total aluminium: across the H-MOR steaming series of Xu et al. the bulk Si/Al moved only from 9.1 to 12.5 while the framework ratio determined by ^{29}Si NMR moved from 8.74

DOI: 10.54254/2755-2721/2026.38490

to 40.65 [9]. ^{27}Al MAS NMR separates tetrahedral framework Al near 55 ppm from octahedral EFAl near 0 ppm and is the standard tool for distinguishing the two, though its signal intensity is sensitive to hydration state and to quadrupolar broadening of distorted sites, so comparison against bulk elemental analysis after digestion is advisable.

Channel-resolved acid quantification is available in three independent forms: pyridine-preadsorbed NH_3-TPD, which exploits the exclusion of pyridine from the 8-MR [8]; CD_3CN with ^{1}H MAS NMR, which splits the Brønsted signal into 12.3 ppm for the 8-MR T3 site and 10.2 ppm for the 12-MR sites [10]; and infrared deconvolution of the 3610 and 3590 cm^{-1} bands [9, 23]. Reported parent 8-MR to 12-MR ratios range from 48:52 [8] to 28:72 [10] and should be measured for each material.

For textural characterisation, XRD relative crystallinity is insensitive at the relevant scale — samples spanning Si/Al 7.5 to 40 gave almost identical powder patterns [15], and crystallinity rose from 100 to 103.5 in one steaming series while micropore volume fell 18% [24]. Nitrogen physisorption at 77 K is diffusion-limited within the side pocket, whereas argon at 87 K with a Horváth–Kawazoe treatment resolves the two micropore populations and n-nonane pre-adsorption quantifies pocket enlargement [11]. Performance evaluation should follow the criteria of Section 2.2.

5. Conclusions and outlook

Research over the past decade has established that at DAC-relevant concentration the 8-MR/O33 environment governs CO_2 uptake in mordenite rather than total cation content, that cation charge density and hydration energy determine which cations can occupy that environment, and that channel-selective dealumination is achievable by several routes. Cation site-protection combined with steaming currently gives the largest quantified discrimination, in-situ proton generation the most complete structural evidence, and conventional acid leaching the most accessible degree control. The four strategy families are compared in Table 2.

Several challenges remain. The location of adsorbed water within the two channel systems has not been determined with the specificity achieved for CO_2, so the relative contribution of 12-MR and 8-MR cations to water uptake is unknown. The net effect of dealumination on humid performance likewise remains to be established, since raising Si/Al lowers framework polarity while simultaneously generating silanol defects, removing CO_2-binding cations, retaining pore-blocking EFAl and enlarging the side pocket. Reported results for steaming of unprotected H-MOR differ between studies conducted at different steam partial pressures, and the effect of steam concentration has not been examined as an independent variable.

Future work would benefit from combining the three capabilities that have so far been demonstrated separately: channel-resolved dealumination developed within the catalysis community, textural resolution of the side pocket by high-resolution argon physisorption, and evaluation of cyclic working capacity under humid DAC conditions. Applying channel-selective treatment to a cation-form mordenite, with concentration- and pH-matched non-chelating controls to separate the contributions of chelation and acid leaching, and characterising the products in a manner that is simultaneously framework-resolved, channel-resolved and textural, would allow the relationship between the position of aluminium removal and humid CO_2 performance to be established directly.

References

[1] Sanz-Pérez, E. S., Murdock, C. R., Didas, S. A., & Jones, C. W. (2016). Direct capture of CO2 from ambient air. *Chemical Reviews, 116*, 11840-11876.

DOI: 10.54254/2755-2721/2026.38490

[2] Siegelman, R. L., Kim, E. J., & Long, J. R. (2021). Porous materials for carbon dioxide separations. *Nature Materials, 20*, 1060-1072.
[3] Lyadov, I., & Lusardi, M. (2025). Characterization of K-MER and 13X zeolites for humid direct air capture of CO2 under equilibrium and cycling conditions. *Chemical Engineering Journal, 524*, 168648.
[4] Goyal, N., Hu, Y.-b., Li, F., & Yuan, B. (2025). Advances in hydrophobic physisorbents for CO2 capture from humid flue gas and direct air. *Separation and Purification Technology, 362*, 131729.
[5] Fu, D., Park, Y., & Davis, M. E. (2022). Confinement effects facilitate low-concentration carbon dioxide capture with zeolites. *Proceedings of the National Academy of Sciences, 119*, e2211544119.
[6] Kong, X., Wu, J., Ming, S., Cheng, C., Wu, Q., Wang, Y., Li, X., Pang, L., Guo, Y., & Li, T. (2025). Unveiling specific CO2 trapping sites within MOR zeolite for promoting direct air capture of CO2. *Chemical Engineering Journal, 506*, 159855.
[7] Lee, S., Lee, H., Hwang, H., Seoung, D., Kim, H., Kim, P., & Lee, Y. (2025). Relationship between electronegativity of the extra-framework cations and adsorption capacity for CO2 gas on mordenite framework. *Inorganic Chemistry, 64*, 903-910.
[8] Xue, H., Huang, X., Zhan, E., Ma, M., & Shen, W. (2013). Selective dealumination of mordenite for enhancing its stability in dimethyl ether carbonylation. *Catalysis Communications, 37*, 75-79.
[9] Xu, F., Lv, J., Chen, C., Hong, Z., Zhao, G., Miao, L., Yang, W., & Zhu, Z. (2022). Effect of steam treatment on the properties of mordenite and its catalytic performance in a DME carbonylation reaction. *Industrial & Engineering Chemistry Research, 61*, 1258-1266.
[10] Xing, Y. et al. (2025). Targeted dealumination via in situ activation of persulfate in size-selective zeolite channels. *The Journal of Physical Chemistry Letters, 16*, 5878-5886.
[11] Benamar, M., Sachse, A., Miqueu, C., & Batonneau-Gener, I. (2024). Textural characterization of zeolites with complex pore systems: The case of dealuminated mordenite zeolites. *Materials Today Chemistry, 36*, 101974.
[12] Li, X., Shen, W., Sun, H., Meng, L., Wang, B., Zhan, C., & Zhao, B. (2020). Theoretical studies on carbon dioxide adsorption in cation-exchanged molecular sieves. *RSC Advances, 10*, 32241-32248.
[13] Zukal, A., Pulido, A., Gil, B., Nachtigall, P., Bludský, O., Rubeš, M., & Čejka, J. (2010). Experimental and theoretical determination of adsorption heats of CO2 over alkali metal exchanged ferrierites with different Si/Al ratio. *Physical Chemistry Chemical Physics, 12*, 6413-6422.
[14] Silaghi, M.-C., Chizallet, C., Sauer, J., & Raybaud, P. (2016). Dealumination mechanisms of zeolites and extra-framework aluminum confinement. *Journal of Catalysis, 339*, 242-255.
[15] Nagano, J., Eguchi, T., Asanuma, T., Masui, H., Nakayama, H., Nakamura, N., & Derouane, E. G. (1999). 1H and 129Xe NMR investigation of the microporous structure of dealuminated H-mordenite probed by methane and xenon. *Microporous and Mesoporous Materials, 33*, 249-256.
[16] Yoshioka, T. et al. (2022). Dealumination of small-pore zeolites through pore-opening migration process. *Science Advances, 8*, eabo3093.
[17] Giudici, R., Kouwenhoven, H. W., & Prins, R. (2000). Comparison of nitric and oxalic acid in the dealumination of mordenite. *Applied Catalysis A: General, 203*, 101-110.
[18] Reule, A. A. C., Sawada, J. A., & Semagina, N. (2017). Effect of selective 4-membered ring dealumination on mordenite-catalyzed dimethyl ether carbonylation. *Journal of Catalysis, 349*, 98-109.
[19] Babić, V., Koneti, S., Moldovan, S., Debost, M., Gilson, J.-P., & Valtchev, V. (2022). Chromic acid dealumination of zeolites. *Microporous and Mesoporous Materials, 329*, 111513.
[20] Xu, F., Zheng, J., Li, J., & Zhu, Z. (2025). Enhances the activity of mordenite in DME carbonylation reaction by controlling the degree of dealumination. *iScience, 28*, 112102.
[21] Hu, M., Qie, Z., Liu, Z., Lu, X., Bai, S., Lv, L., Wang, Z., Xiang, H., Ou, X., & Zhuang, Y. (2025). Sequential carboxylic acid and ammonium hydroxide treatments for zeolites: Enhancing CO2 adsorption under humid conditions. *Microporous and Mesoporous Materials, 384*, 113465.
[22] Fan, Y., Lin, X., Shi, G., Liu, H., & Bao, X. (2007). Realumination of dealuminated HZSM-5 zeolite by citric acid treatment and its application in preparing FCC gasoline hydro-upgrading catalyst. *Microporous and Mesoporous Materials, 98*, 174-181.
[23] Armitage, G. G., & Sunley, J. G. (2015). Selective dealumination of MOR type zeolites. US Patent No. 8,956,588 B2.
[24] Bai, X., Zhang, J., Liu, C., Xu, S., Wei, Y., & Liu, Z. (2023). Solid-state NMR study on the dealumination mechanism of H-MOR zeolite by high-temperature hydrothermal treatment. *Microporous and Mesoporous Materials, 354*, 112555.
[25] Liu, R., Zeng, S., Sun, T., Xu, S., Yu, Z., & Liu, Z. (2022). Selective removal of acid sites in mordenite zeolite by trimethylchlorosilane silylation. *ACS Catalysis, 12*, 4491–4500.

DOI: 10.54254/2755-2721/2026.38490

[26] Chen, O. I.-F., Liu, C.-H., Wang, K., Borrego-Marin, E., Li, H., Alawadhi, A. H., Navarro, J. A. R., & Yaghi, O. M. (2024). Water-enhanced direct air capture of carbon dioxide in metal-organic frameworks. *Journal of the American Chemical Society, 146*, 2835–2844.

[27] Liu, Z., Shi, G., Sun, S., Wang, Y., Shang, J., Hu, S., Deng, W., Fu, C., Liu, C., Wang, X., Qi, T., & Hu, G. (2026). Combined aperture widening and strong polarization in Li+-exchanged mordenite for efficient direct air capture of CO2. *Chemical Engineering Journal, 530*, 173599.